

Fluid	Dry Air (gas)	Methane (gas)	Water (liquid)	Ethanol (liquid)
Density, ρ (kg/m ³)	1.21	0.669	988	789
Dynamic viscosity, μ (kg/m-s)	1.82×10^{-5}	1.10×10^{-5}	1.00×10^{-3}	9.67×10^{-4}
Kinematic viscosity, ν (m ² /s)	1.51×10^{-5}	1.65×10^{-5}	1.00×10^{-6}	1.23×10^{-6}
Surface tension w/ air, σ (N/m)	---	---	7.28×10^{-2}	2.28×10^{-2}
Speed of sound, a (m/s)	343	445	1482	1200
Specific heat, c_p (J/kg-K)	1010	2220	4190	2440
Gas constant, R_g (J/kg-K)	287	518	---	---
Mass diffusivity, Θ (m ² /s)	---	1.55×10^{-5} in air	---	1.12×10^{-9} in water
Schmidt Number, Sc	---	1.06 in air	---	1100 in water
Thermal conductivity, k (J/m-K-s)	2.57×10^{-2}	3.35×10^{-2}	5.98×10^{-1}	1.68×10^{-1}
Prandtl Number, Pr	0.717	0.729	7.01	14.04

Table A.1 Properties of fluids at normal temperature and pressure (NTP: T= 293 K=20° C and p=101,320 N/m²) based on data from Schlichting & Gresten (2000), White, (1991), King, *et al.* (1965), Lide (2005).

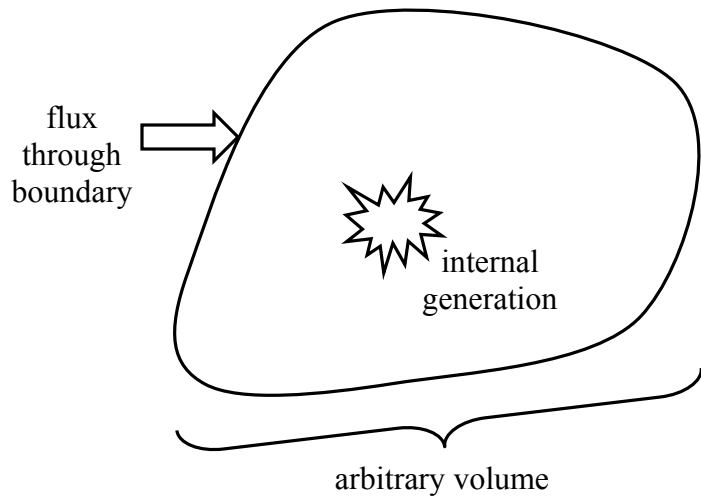


Fig. A.1 Reynolds Transport Theorem for an arbitrary volume where total change in time of a quantity is equal to its flux through the boundary plus any internal generation.

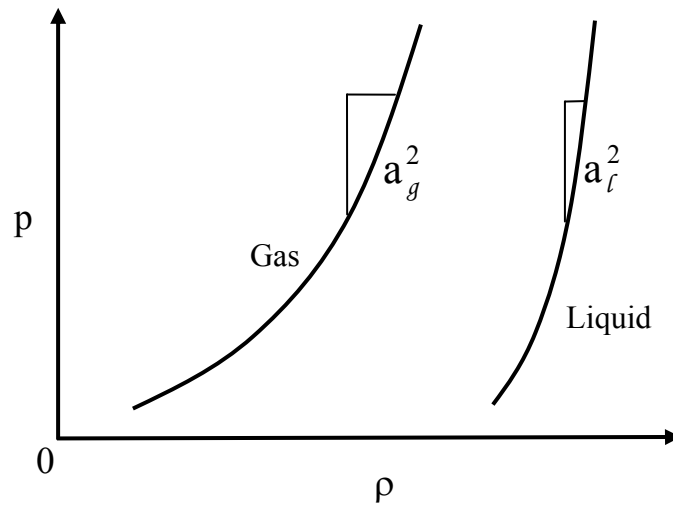
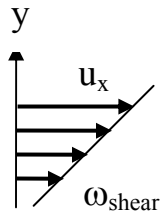


Fig. A.2 Qualitative isentropic pressure-density relationship for a calorically perfect gas and for a liquid governed by the Tait equation of state.

a)



b)

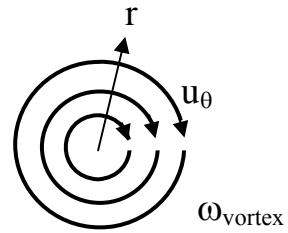


Fig. A.3 Schematic of constant vorticity flows: a) linear shear and b) simple vortex.

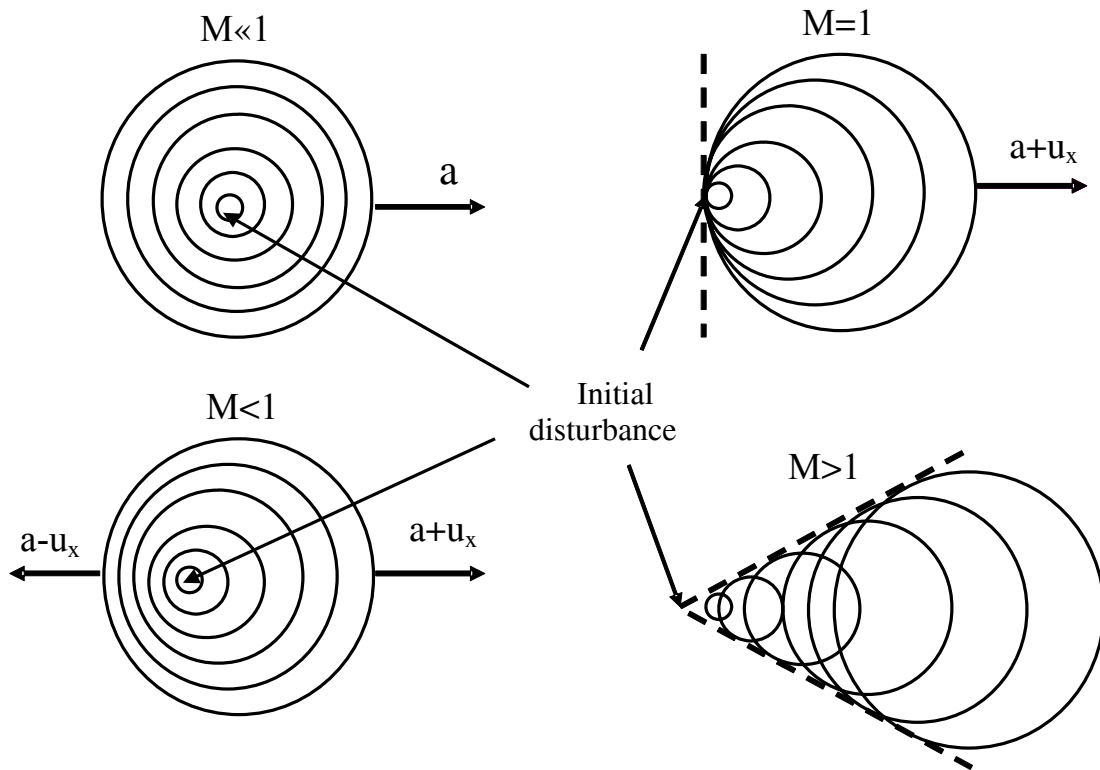


Fig. A.4 Schematic of sound waves traveling from a small initial disturbance under various Mach number regimes.

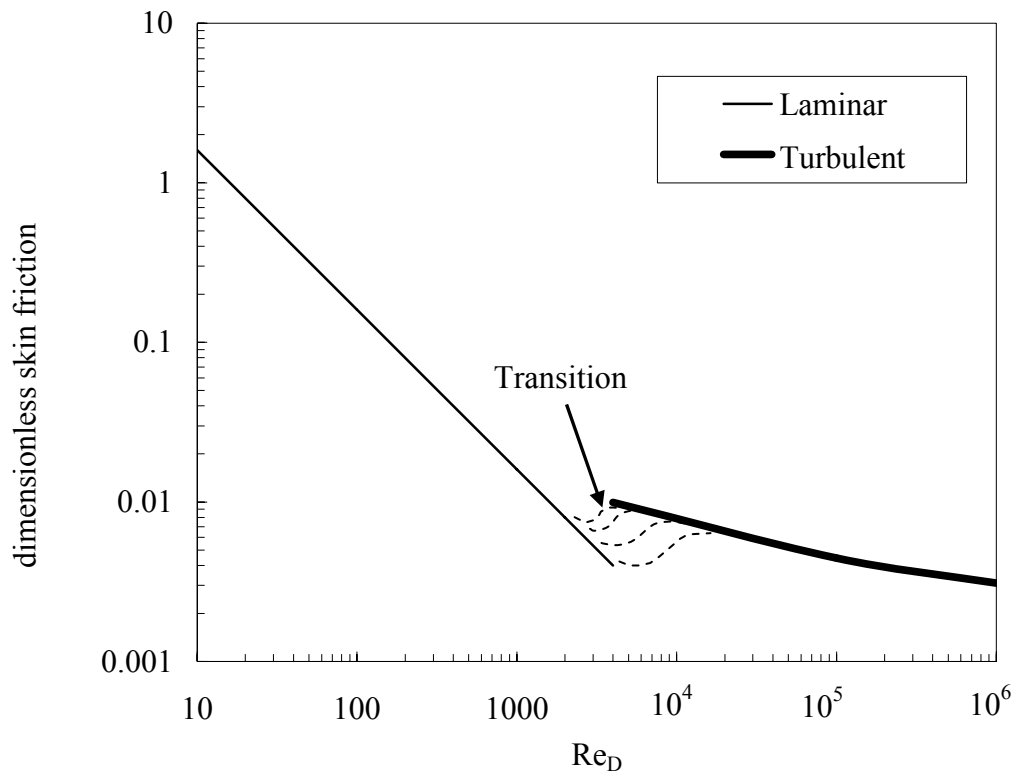


Fig. A.5 Friction coefficient for a smooth fully-developed pipe flow as a function of pipe Reynolds number for laminar flow ($Re_D < Re_{D,crit}$), transitional flow ($Re_{D,crit} < Re_D < Re_{D,turb}$), and turbulent flow ($Re_D > Re_{D,turb}$).

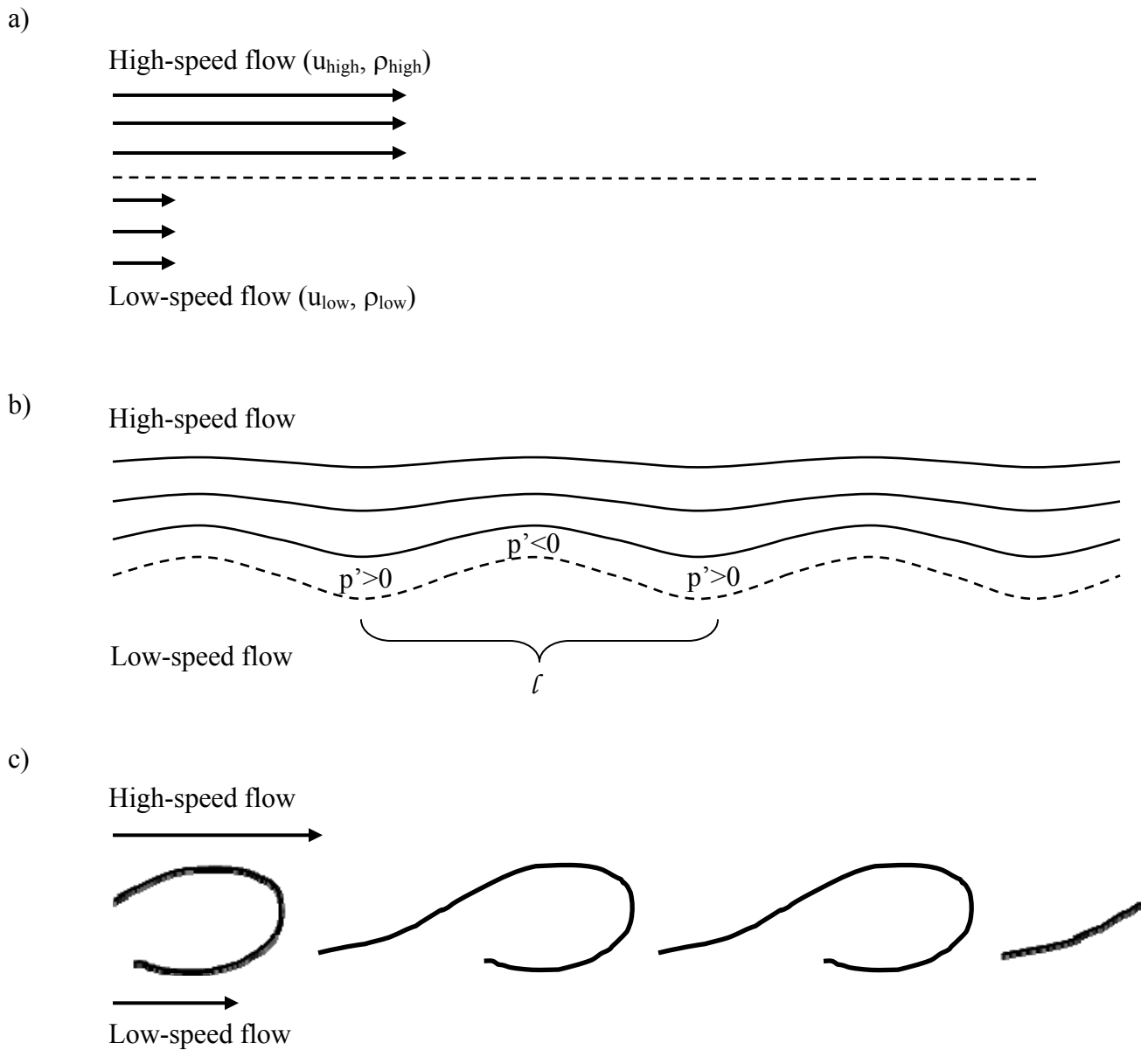


Fig. A.5X Kelvin-Helmholtz instability for two flows moving past each other with different speeds (and potentially different densities): a) initial conditions with two different flow speeds without any perturbations and uniform pressure (p_0) throughout, b) interface perturbed by a wavelength (ℓ) and associated impact on high-speed flow streamlines and perturbed pressure field ($p' = p - p_0$), and c) schematic of the eddy and braid flow after perturbations are amplified and interact.

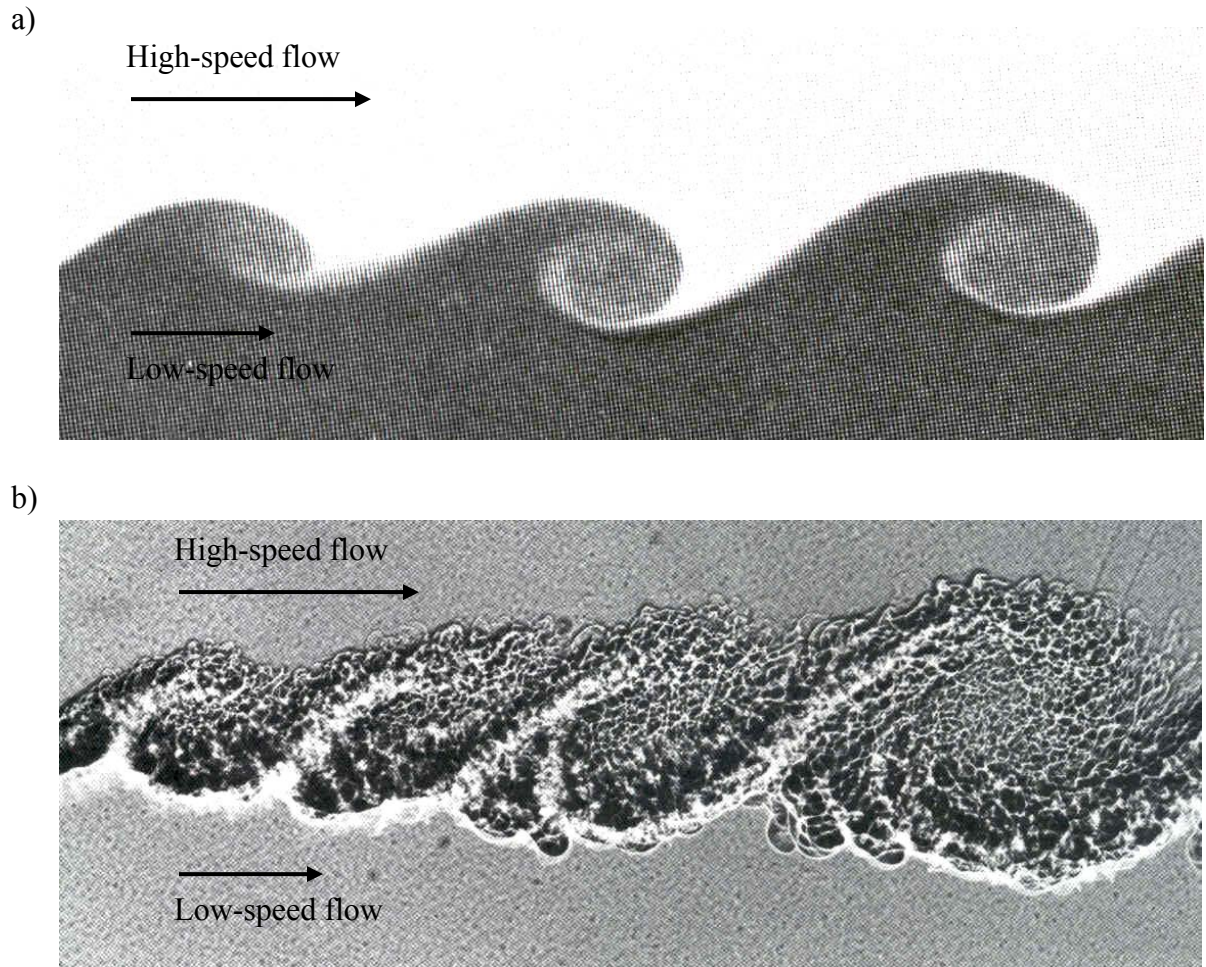


Fig. A.6 Mixing-layer images: a) at transitional conditions (Van Dyke, 1982), and b) turbulent conditions (Van Dyke, 1982).

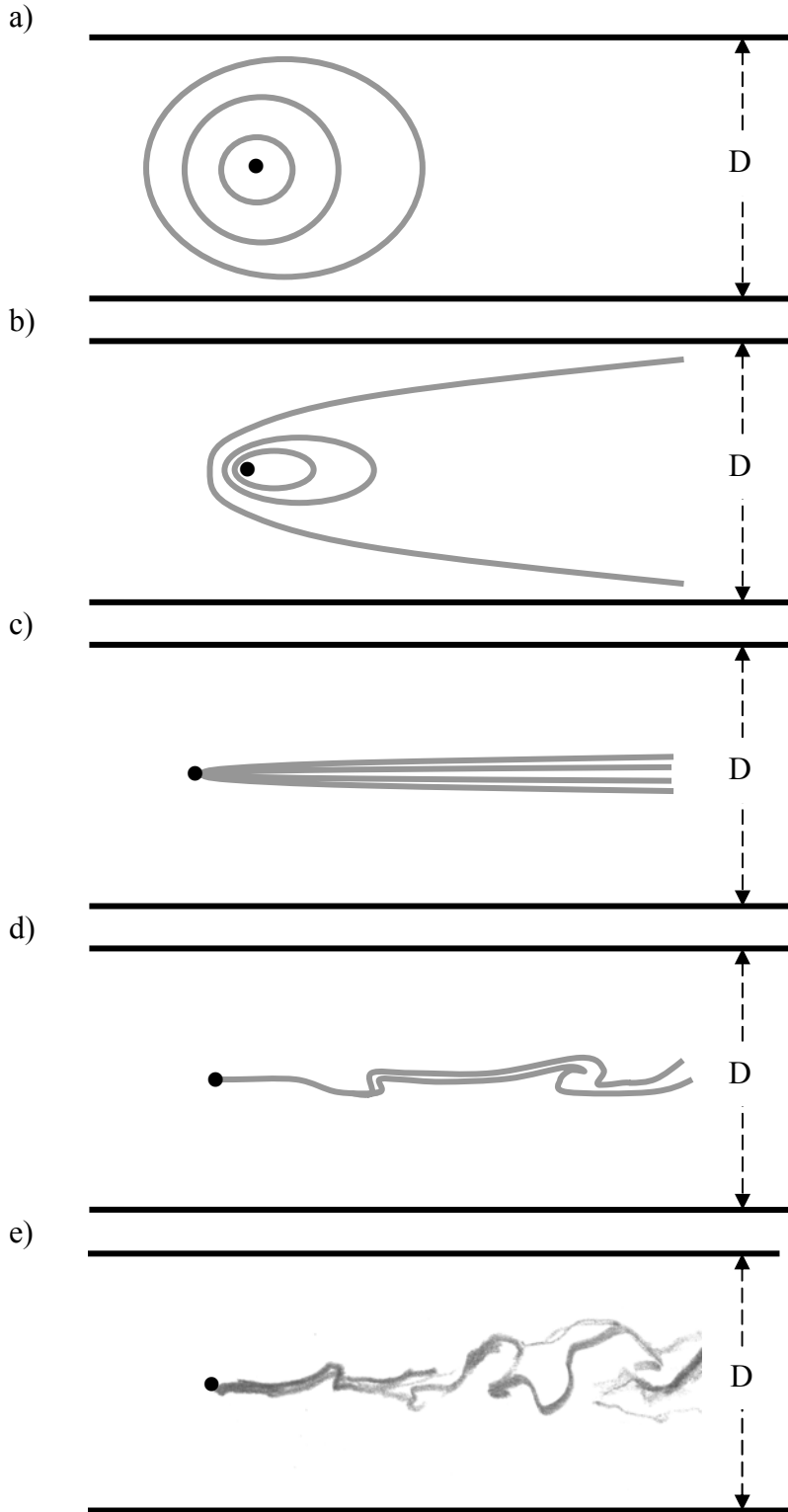
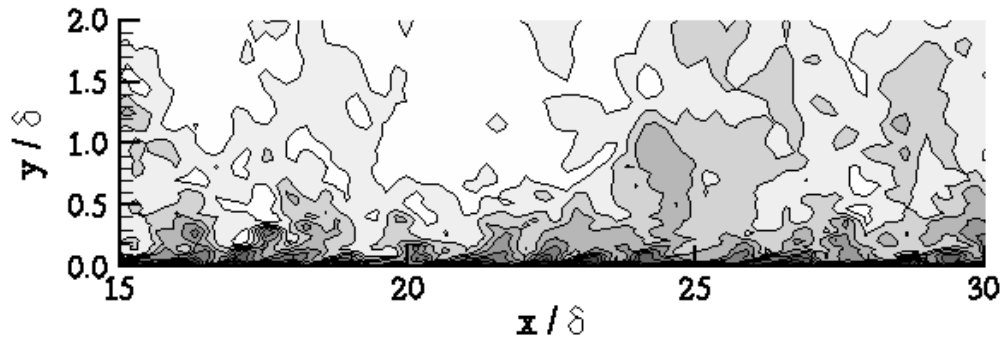


Fig. A.7 Illustration of mass diffusion of fluid elements released in the center of a pipe (black dot) where flow is left-to-right and Schmidt number is approximately unity. Sketches of concentration iso-contours are shown for: a) $Re_D \ll 1$, b) $Re_D \sim 1$, c) $Re_D \gg 1$ but still laminar, d) transitional flow, and e) turbulent flow.

a)



b)

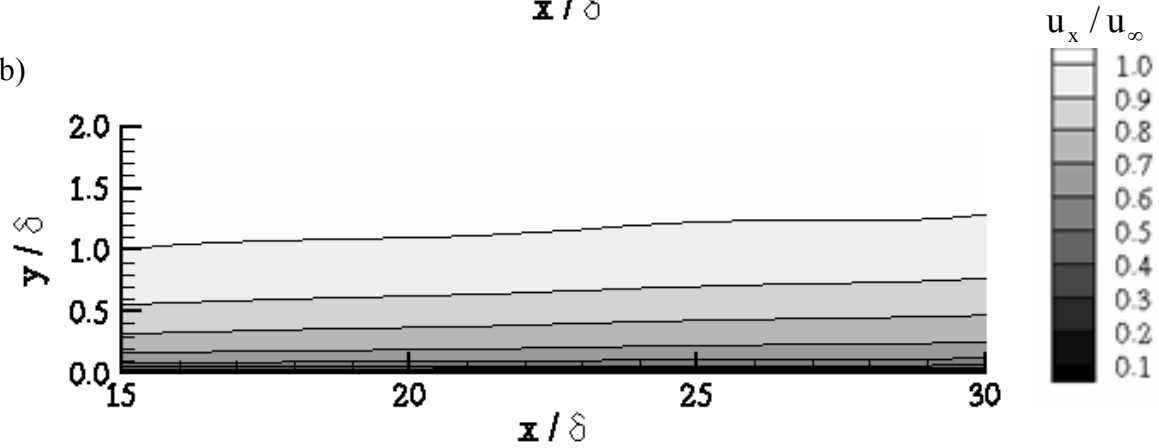
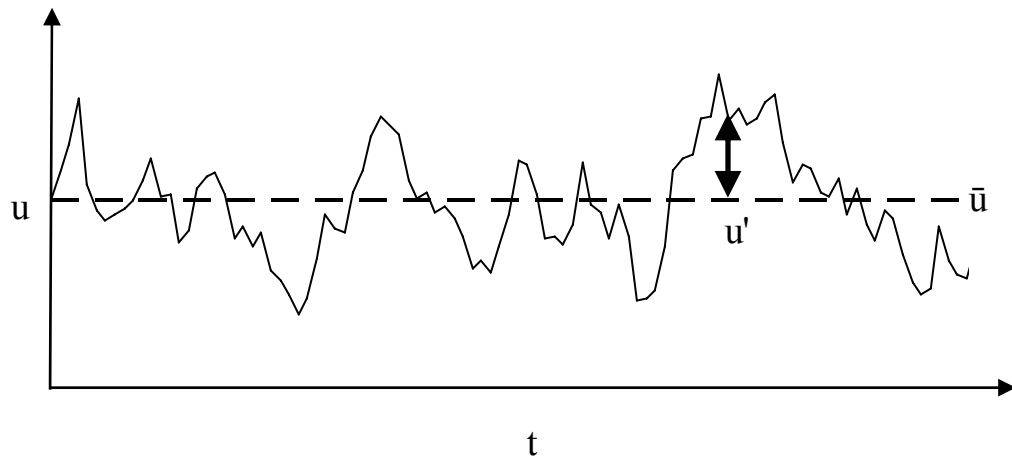


Fig. A.8 Different representations of a turbulent boundary layer from Dorgan & Loth (2004) where x is the streamwise direction and y is normal to the wall: a) two-dimensional slice of the instantaneous three-dimensional velocity field, and b) the two-dimensional steady time-average velocity field. The mean boundary layer thickness (δ) is the y -location where the mean velocity achieves 99% of the free-stream velocity.

a)



b)

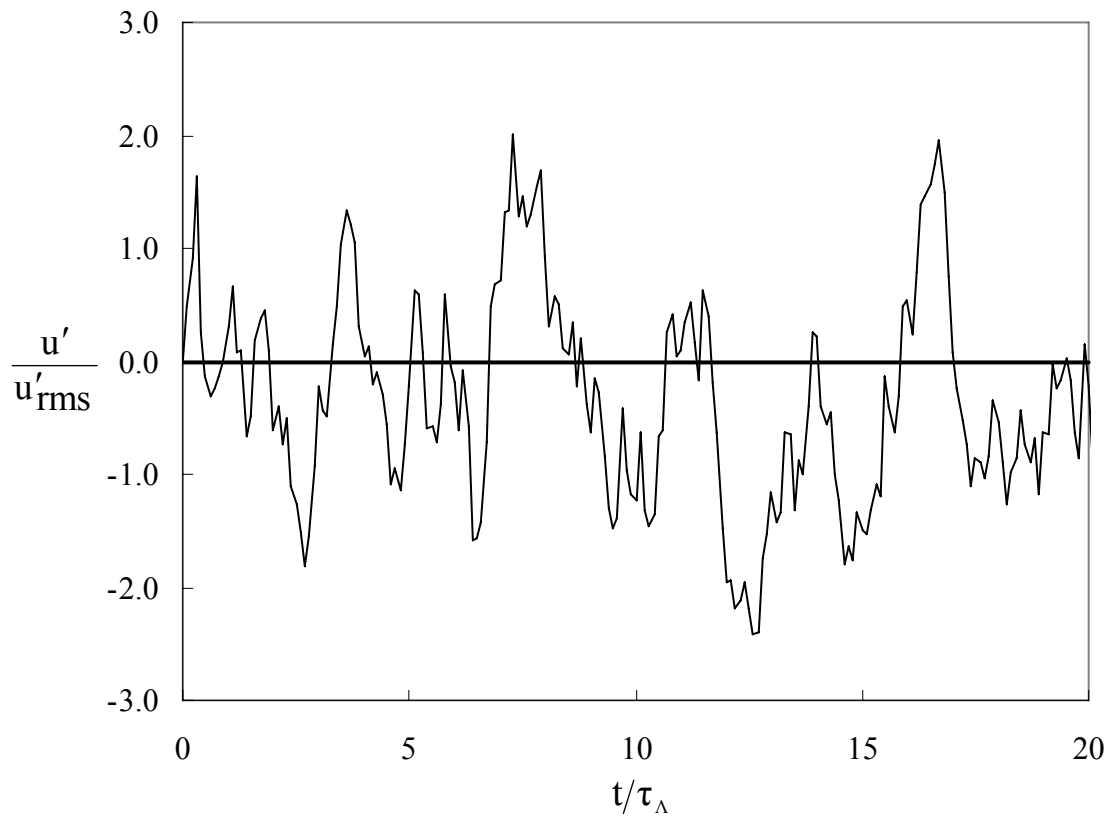


Fig. A.9 Sample time-history of velocity in a turbulent flow: a) instantaneous velocity as a function of time, and b) velocity perturbations scaled with the rms value and time scaled with the turbulent integral scale.

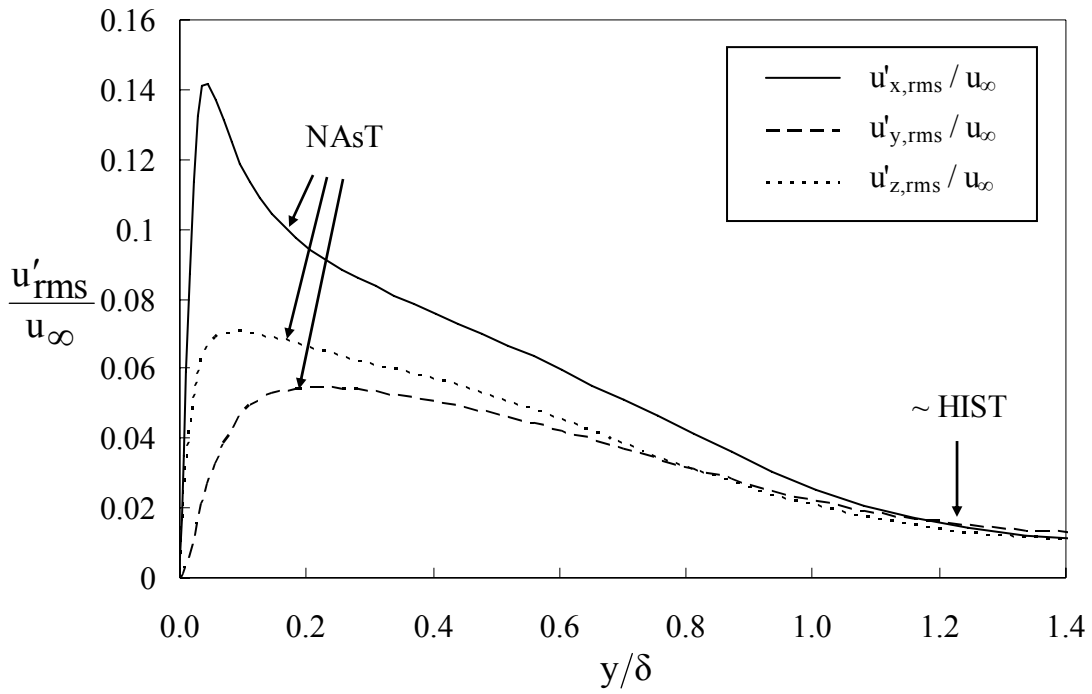


Fig. A.10 Velocity fluctuation distributions in the turbulent boundary layer of Fig. A.7 where δ is the boundary layer thickness (in the y-direction), and u_∞ is the free-stream velocity in the x-direction (Dorgan & Loth, 2004).

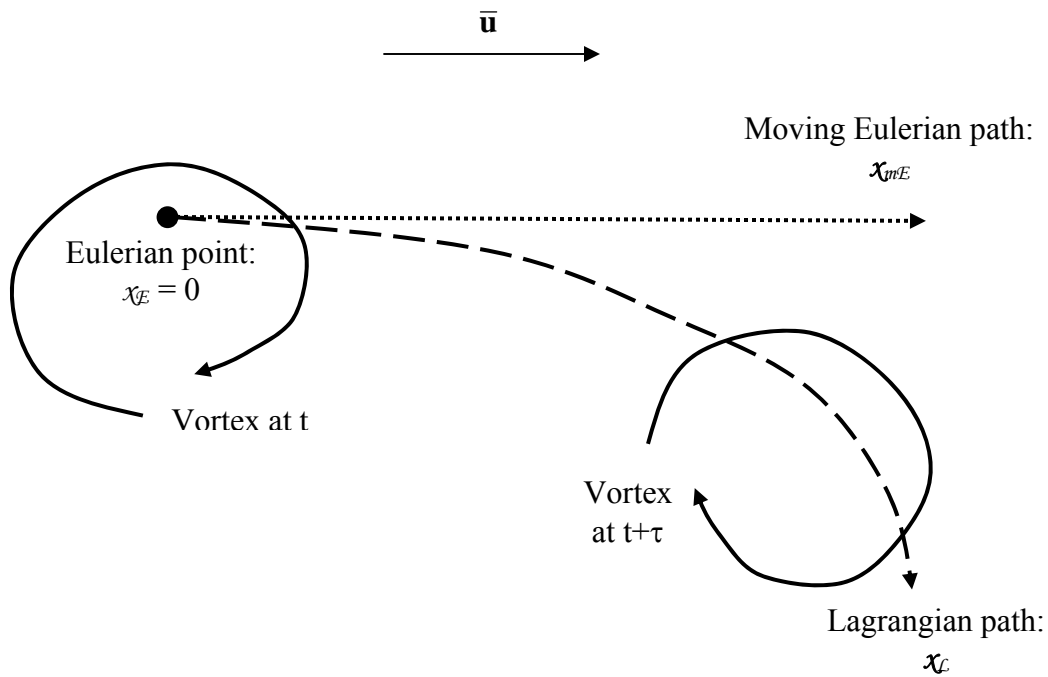


Fig. A.11 Illustration of a flow where the mean velocity is horizontal but the instantaneous velocity happens to include a downward trajectory and shows the three primary reference frames for temporal correlations: a) Eulerian based on a fixed point in time (solid circle), b) Lagrangian based on continuous-phase fluid velocity (long-dash), and c) moving Eulerian based on the mean continuous-phase velocity direction (short-dash).

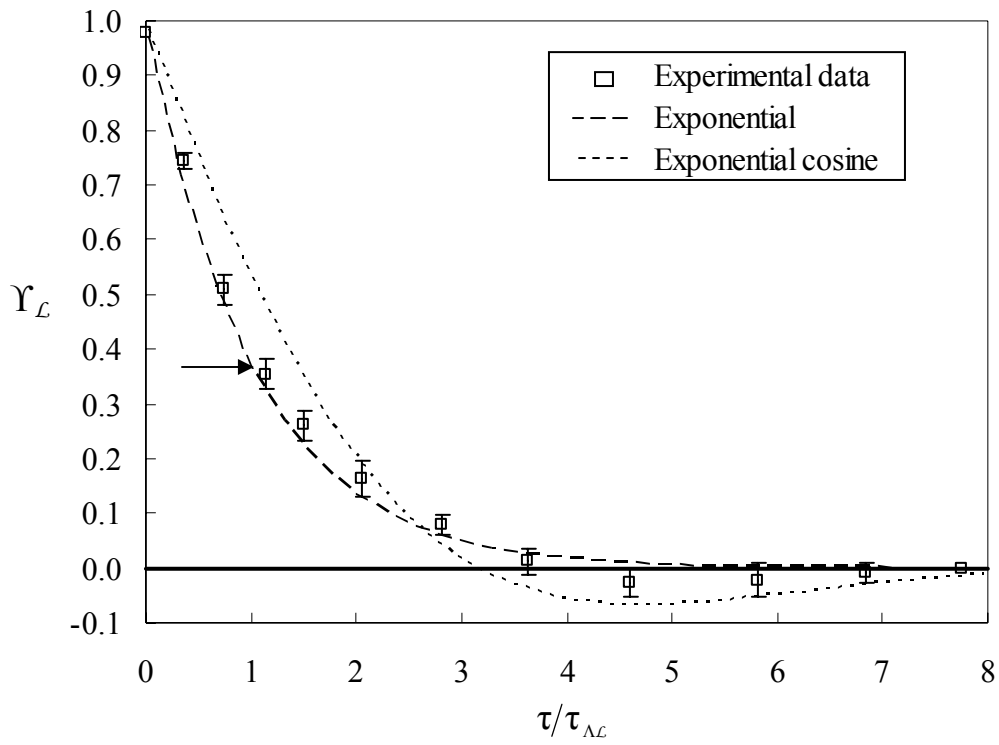


Fig. A.12 Lagrangian correlation coefficient as a function of separation time showing approximate curves compared to experimental data downstream of grid-generated turbulence which is approximately homogeneous and isotropic (Snyder & Lumley, 1971). The arrow indicates a correlation of $1/e$ which defines τ_{Λ} for an exponential decay.

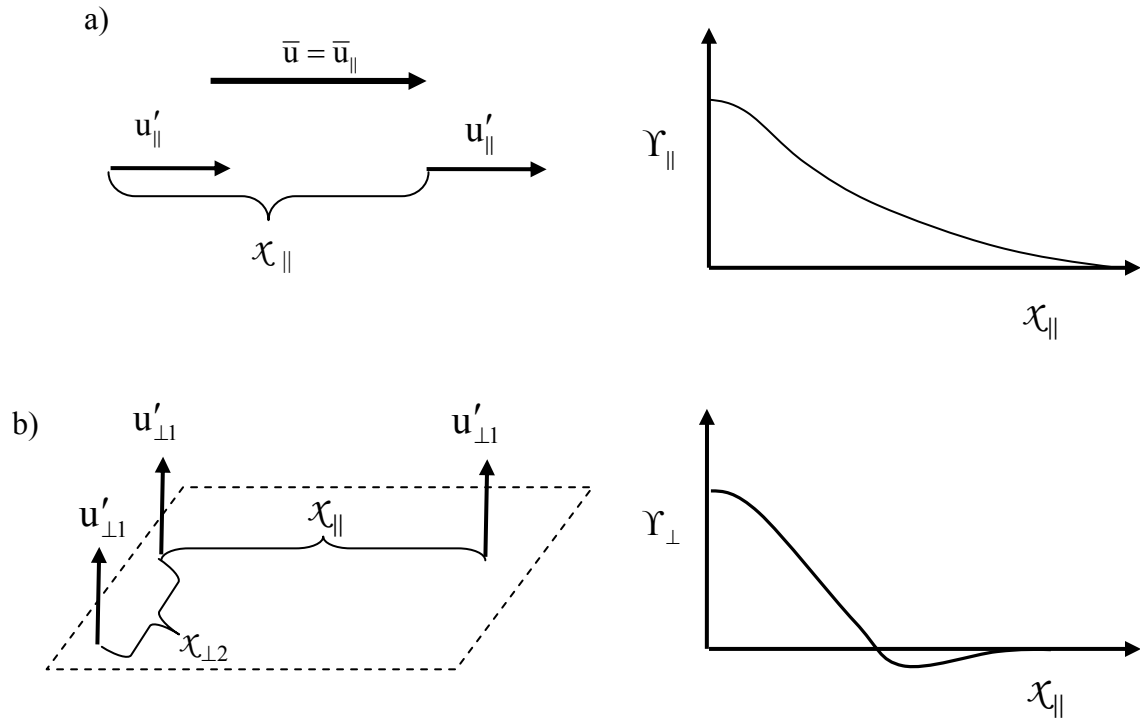
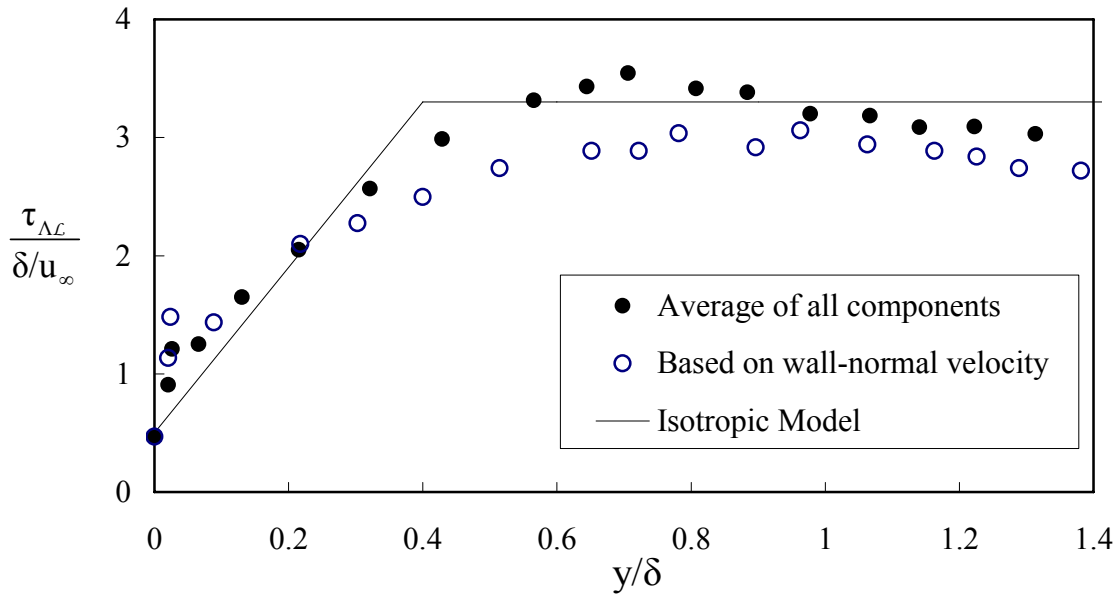


Fig. A.13 Diagram of longitudinal spatial shift of: a) schematic of the longitudinal velocity perturbations and associated correlation function, and b) schematic of the lateral velocity perturbations with a surface along the mean flow (shown in dashed lines) and associated spatial correlation function whereby a negative loop is produced.

a)



b)

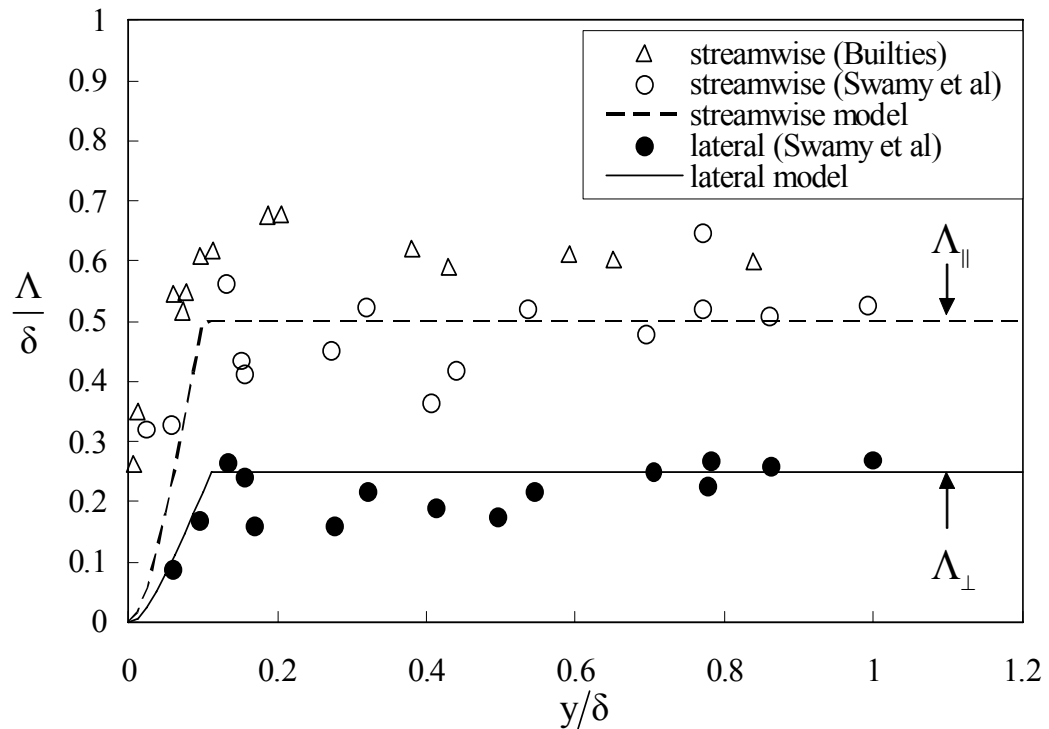


Fig. A.14 Integral scales of a turbulent boundary layer normalized the domain scales (boundary layer thickness and free-stream velocity): a) integral time-scales based on Lagrangian fluid-tracer trajectories at $Re_\delta=4,500$ (Bocksell & Loth, 2006), and b) Eulerian measurements of streamwise integral length-scale at $Re_\delta \approx 27,000$ (Bultjes, 1975) and $Re_\delta \approx 7,000-17,000$ (Swamy *et al.* 1979).

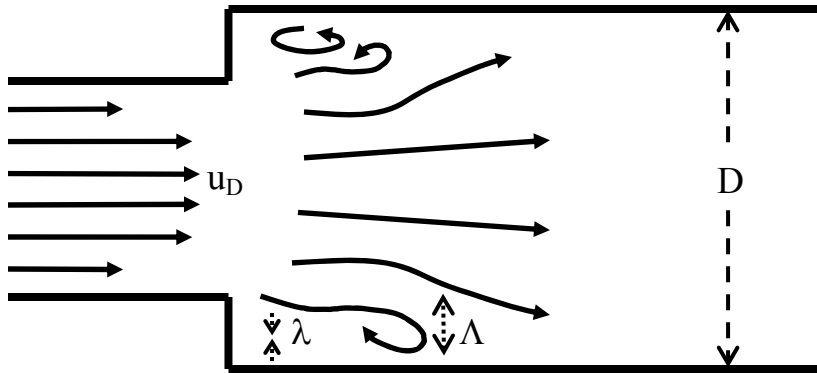


Fig. A.15 Flow in an expanding duct showing various length-scales of the continuous-phase flow including macroscopic length-scale based on a duct diameter (D) as well as an integral length scale (Λ) and a Kolmogorov length scale (λ) based on local turbulent flow features.

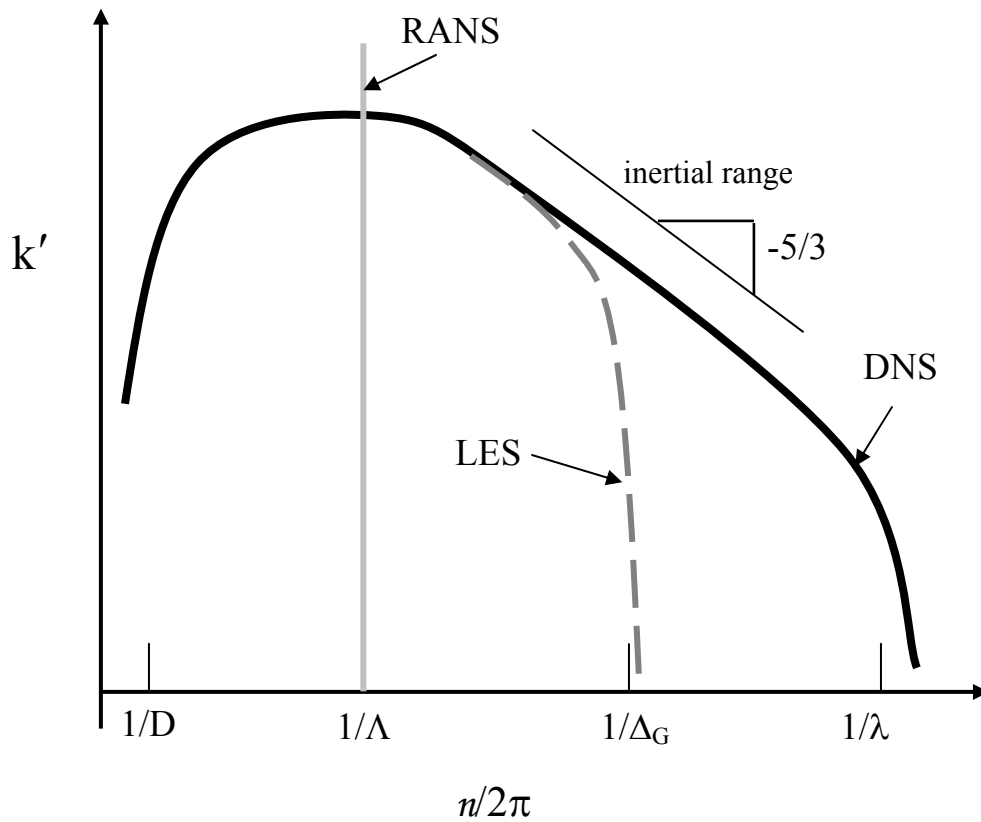


Fig. A.16 Schematic of the turbulence energy spectrum on a log-log scale, where the Reynolds number is presumed to be high enough for an inertial sub-range to be present. Also shown are wave numbers captured by RANS (a single length-scale), LES (ranging from domain length-scale down to a sub-grid length scale), and DNS approaches (all scales).

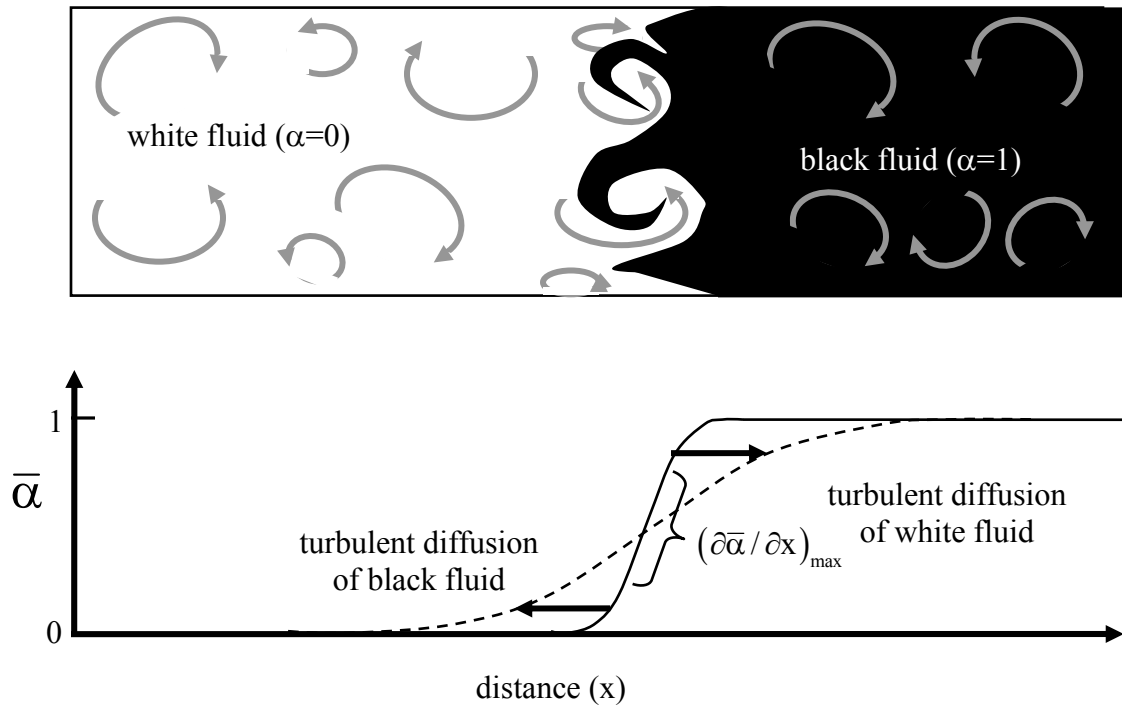


Fig. A.17 Turbulent diffusion an immiscible (no molecular diffusion) black fluid concentration: a) instantaneous concentration spreading by turbulent eddies, and b) a vertically-averaged concentration at two different times where spreading rate is in the opposite direction of the concentration gradient.

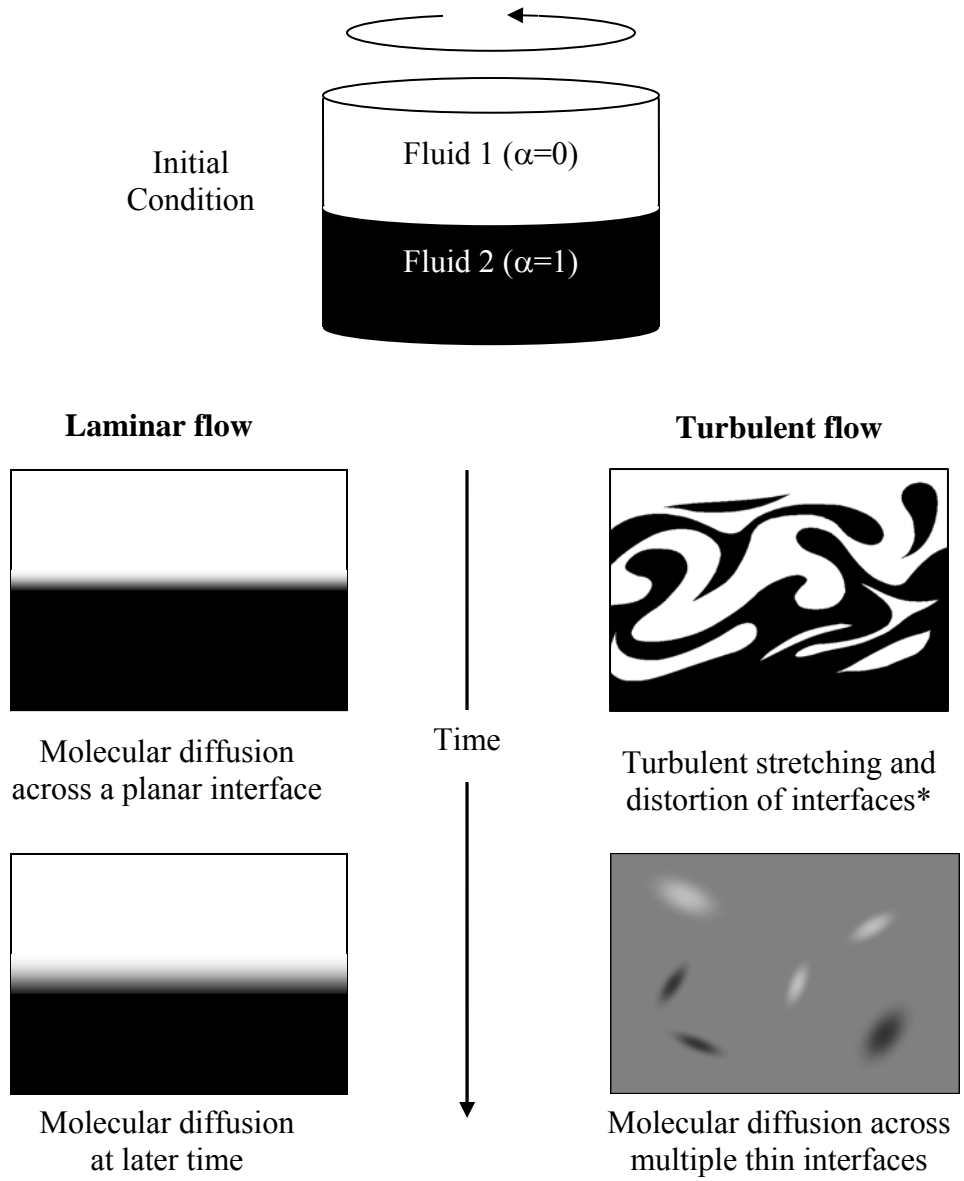


Fig. A.18 Illustration of overall mass diffusion when stirring miscible fluids, e.g., cream on top of coffee, comparing laminar and turbulent conditions.

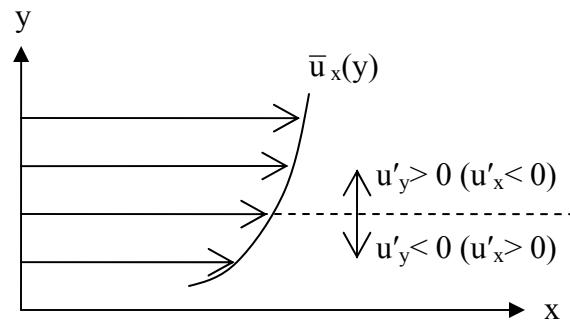


Fig. A.19 Momentum transfer due to turbulent velocity fluctuations in a shear layer with $\partial \bar{u}_x / \partial y > 0$ which results in $\overline{u'_x u'_y} < 0$.

Flow Condition	Flow Reynolds #	Continuous-Phase Momentum Eqs.
Steady Creeping Flow	$Re_D \ll 1$	$0 = \rho_f g_i - \partial p / \partial x_i + \mu_f \partial^2 u_i / \partial x_j \partial x_j$
Steady Laminar Flow	$Re_D < Re_{crit}$	$\rho_f u_j \partial u_i / \partial x_j = \rho_f g_i - \partial p / \partial x_i + \mu_f \partial^2 u_i / \partial x_j \partial x_j$
Transitional Flow	$Re_{crit} < Re_D < Re_{turb}$	$\rho_f \partial u_i / \partial t + \rho_f u_j \partial u_i / \partial x_j =$ $\rho_f g_i - \partial p / \partial x_i + \mu_f \partial^2 u_i / \partial x_j \partial x_j$
Turbulent Flow (DNS)	$Re_D > Re_{turb}$	<i>Same as for transitional flow (above)</i>
Turbulent Flow (LES)	$Re_D > Re_{turb}$	$\rho_f \partial \bar{u}_i / \partial t + \rho_f \bar{u}_j \partial \bar{u}_i / \partial x_j + \rho_f \partial (\overline{u'_i u'_j}) / \partial x_j =$ $\rho_f g_i - \partial \bar{p} / \partial x_i + \mu_f \partial^2 \bar{u}_i / \partial x_j \partial x_j$ <i>where $(\bar{\quad})$ is a spatially-filtered quantity</i>
Turbulent Flow (RANS)	$Re_D > Re_{turb}$	$\rho_f \bar{u}_j \partial \bar{u}_i / \partial x_j + \rho_f \partial (\overline{u'_i u'_j}) / \partial x_j =$ $\rho_f g_i - \partial \bar{p} / \partial x_i + \mu_f \partial^2 \bar{u}_i / \partial x_j \partial x_j$ <i>where $(\bar{\quad})$ is a time-averaged quantity</i>

Table A.2 Forms of the continuous-flow incompressible Navier-Stokes momentum equations, assuming no effect from the particles (i.e. assuming one-way coupling), where Re_{crit} corresponds to the Reynolds number at which the flow begins to become transitional and Re_{turb} corresponds to the Reynolds number at which the flow becomes fully turbulent.

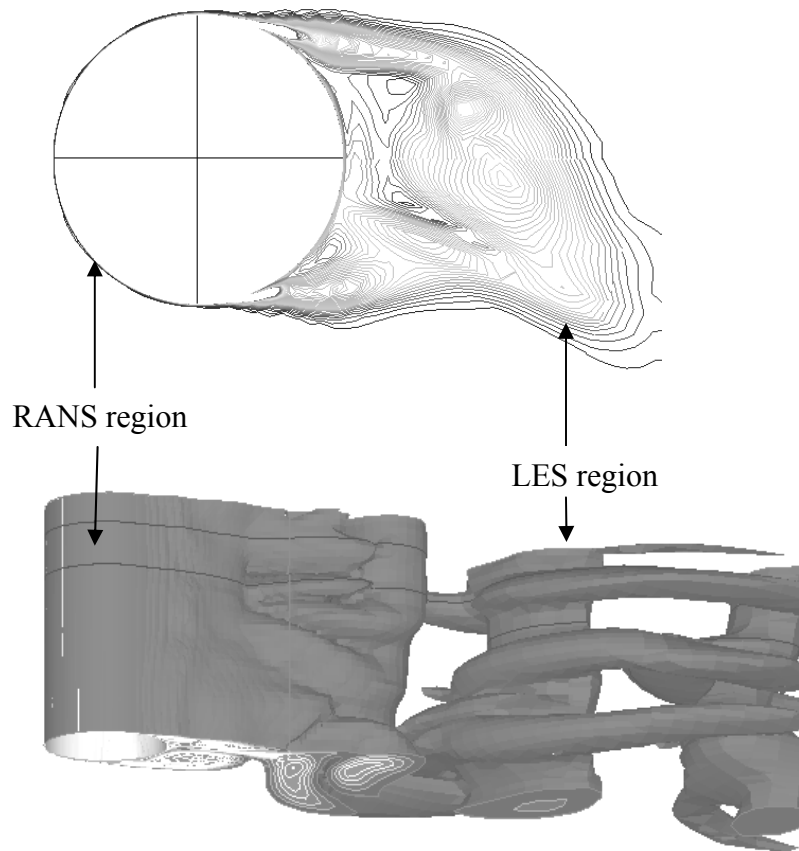


Fig. A.20 Hybrid RANS/LES simulation for flow over a cylinder at Reynolds number of 3×10^6 showing instantaneous cross-sectional and span-wise views.

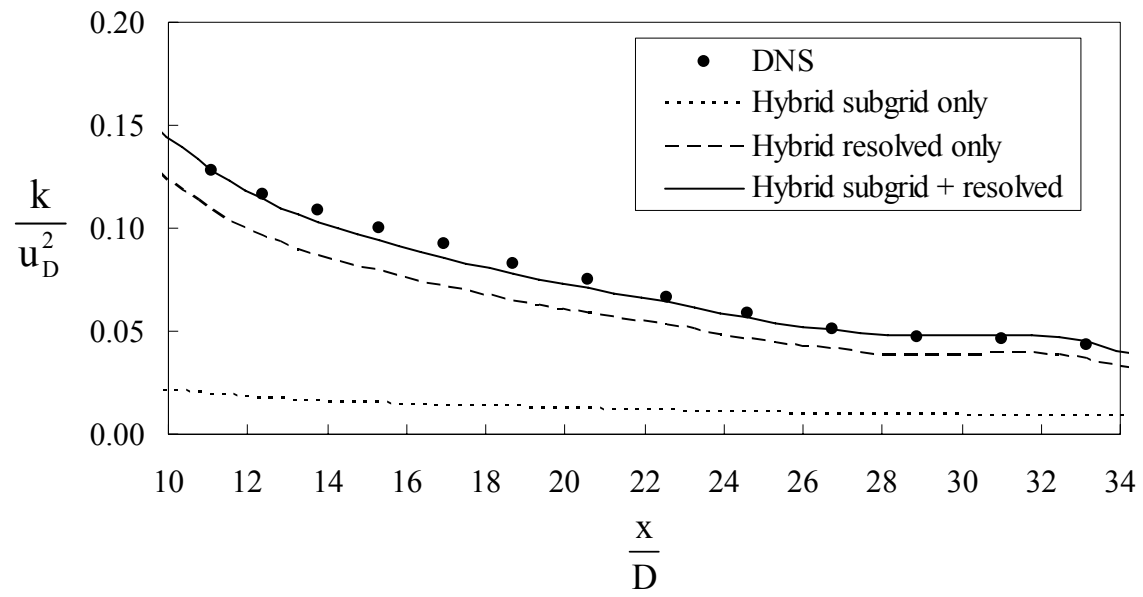


Fig. A.21 Predictions of turbulent kinetic energy along centerline of a cylinder wake (with $Re_D=800$) based on DNS and the Nichols-Nelson hybrid model (Rybalko *et al.* 2008).